ACSNANO

www.acsnano.org

ARTICLE

Structural Colors Enabled by Lattice Resonance on Silicon Nitride Metasurfaces

Jhen-Hong Yang, Viktoriia E. Babicheva, Min-Wen Yu, Tien-Chang Lu, Tzy-Rong Lin, and Kuo-Ping Chen*

Cite This: *ACS Nano* 2020, 14, 5678−5685

Read Online

ACCESS | Metrics & More | Article Recommendations | Supporting Information

ABSTRACT: **Artificial color pixels based on dielectric Mie resonators are appealing for scientific research as well as practical design. Vivid colors are imperative for displays and imaging. Dielectric metasurface-based artificial pixels are promising candidates for developing flat, flexible, and/or wearable displays. Considering the application feasibility of artificial color pixels, wide color gamuts are crucial for contemporary display technology. To achieve a wide color gamut, ensuring the purity and efficiency of nanostructure resonance peaks in the visible spectrum is necessary for structural color design. Low-loss dielectric materials are suitable for achieving vivid colors with structural color pixels. However, high-order Mie resonances prevent color pixels based on dielectric metasurfaces from efficiently generating highly saturated colors. In particular, fundamental Mie resonances (electric/magnetic dipole) for red can result in not only a strong resonance peak at 650 nm but also high-order Mie resonances at shorter wavelengths, which reduces the saturation of the target color. To address these problems, we fabricated silicon nitride metasurfaces on quartz substrates and applied Rayleigh anomalies at relatively short wavelengths to successfully suppress high-order Mie resonances, thus creating vivid color pixels. We performed numerical design, semianalytic considerations, and experimental proof-of-concept examinations to demonstrate the performance of the silicon nitride metasurfaces. Apart from traditional metasurface designs that involve transmission and reflection modes, we determined that lateral light incidence on silicon nitride metasurfaces can provide vivid colors through long-range dipole interactions; this can thus extend the applications of such surfaces to eyewear displays and guided-wave illumination techniques.**

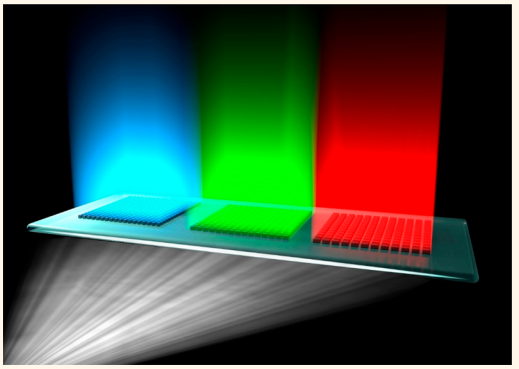

KEYWORDS: *high-refractive-index nanostructures, metasurfaces, color, Mie resonances, lattice resonances, silicon nitride*

Using metasurfaces in image applications has become a crucial subject.[1−4] A wide color gamut and high display resolution are desired to achieve an immersive experience. Compared with components that actively generate color (*e.g.*, organic light-emitting diodes), components that generate color passively are more durable. Passive colors arise from light−matter interactions. Dyes and pigments constitute the most commonly used materials for rendering colors; however, they are chemically unstable at high temperatures and bleach when exposed to intense ultraviolet (UV) illumination. In addition, most dyes and pigments are composed of toxic materials. To achieve an environmentally friendly display with a high resolution and long lifetime, plasmonic[4−10] and dielectric metasurfaces with Mie resonances have been proposed and extensively studied.[11−14] However, colors generated by plasmonic nanostructures are marred by high optical loss, which is not conducive to the generation of efficient and highly saturated colors. By contrast, dielectric metasurfaces are characterized by low optical loss and a high refractive index (*e.g.*, TiO_2,[15,16] Si,[17,18] and Ge[19]); they are thus considered suitable candidates for an efficient color generation.[14,20,21] In designing dielectric metasurfaces, controlling the Mie resonances of each meta-atom is crucial.[22−25] Color pixels based on dielectric metasurfaces with Mie resonances have been proposed.[26−29] Nevertheless, color pixels based on such metasurfaces cannot efficiently generate highly saturated colors because of high-order Mie resonances, particularly when Mie resonances are designed for long wavelengths (*e.g.*, red color). To overcome this difficulty and suppress the excitation of high-order Mie resonances, some researchers proposed the use of

Received: January 8, 2020
Accepted: April 16, 2020
Published: April 16, 2020

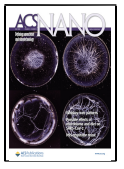

https://dx.doi.org/10.1021/acsnano.0c00185
ACS Nano 2020, 14, 5678−5685

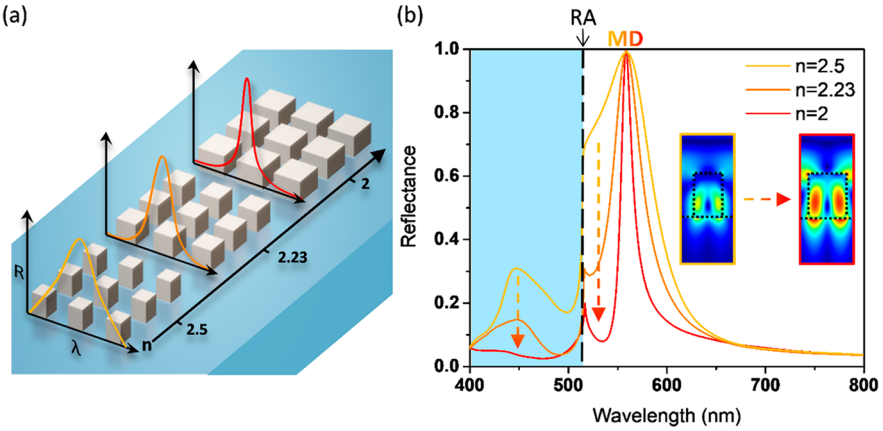

Figure 1. (a) Schematics of dielectric metasurfaces with nanoresonators with different refractive indices. Period (p) and thickness (t) are fixed at 350 and 270 nm, respectively. The width (w) of nanobricks with n = 2.5, 2.23, and 2 is 175, 210, and 255 nm, respectively. The refractive indices of the surrounding medium and substrate are 1 and 1.46, respectively. (b) Reflectance spectra of dielectric metasurfaces with nanoresonators with different refractive indices changing from n = 2.5 to n = 2 (without imaginary part). The RA (black dashed line) corresponding to the substrate (n = 1.46) occurs at the wavelength of 532 nm. The weak coupling effect (no lattice effect) occurs in the region under the RA (light blue shading). Above the RA, the strong coupling effect dominates the reflection in the zero-order diffraction. The insets show the normalized electric field distributions at the MDR wavelength (left and right pictures are for n = 2.5 and n = 2, respectively).

additional layers (antireflection coating) on top of and/or below the Mie resonator.[30] However, the inclusion of additional layers increases the steps in the nanofabrication process and considerably complicates color pixel realization. To address these limitations, we propose and demonstrate the concept of color pixel design for controlling the reflection gamut using Mie resonator arrays on transparent substrates.

RESULTS AND DISCUSSION

Design and Simulation. Nanoparticle lattices facilitate efficient excitation of additional nanostructure resonances, also called lattice resonances, which occur at wavelengths close to Rayleigh anomalies (RAs; wavelengths of diffraction).[31−40] In the design of metasurfaces for display, Mie lattice resonances should be considered because of the coupling effect in array structures. Mie lattice resonances have been demonstrated by Evlyukhin et al.[41,42] in theory and simulation, and they have been demonstrated experimentally and applied in the design of an optical absorber.[43] The excitation of Mie lattice resonances can be influenced by the substrate below the metasurface, which has been studied in detail in the research.[44] Notably, high-order Mie resonances can be suppressed by RAs at relatively short wavelengths. The enhanced coupling can dominate the reflection spectrum, resulting in a single sharp resonance. To produce a high-purity color, combining a fundamental magnetic dipole resonance (MDR) and a Mie lattice resonance is a viable and reasonable approach because no other Mie resonances occur at longer wavelengths. Simultaneously, the contribution of an electric dipole resonance (EDR) to reflection can be suppressed, which is explained as follows.

High-refractive-index dielectrics are suitable for nanoresonators and metasurfaces. Silicon,[29] GaN,[13] TiO_2,[14,45−47] and Si_3N_4[21] have been proposed for designing nanoparticle arrays for use in color imaging. Among these dielectric materials, silicon and GaN have the highest refractive indices. However, GaN is difficult to fabricate, and silicon is marred by a high optical loss at visible wavelengths, which engenders difficulty in producing acceptable green and blue colors. Compared with TiO_2, Si_3N_4 is more suitable for nanostructures that induce magnetic dipole lattice resonances (MDLRs); the superior suitability of Si_3N_4 is attributed to its moderate refractive index. As presented in Figure 1, Si_3N_4 nanoresonators induce a stronger MDLR than TiO_2 nanoresonators do. To explain this, reflection spectra observed for different refractive indices of Mie resonators are compared in this figure. For a fixed period (p) of 350 nm, the quality factor of the MDLR is shown to increase (narrower, thus preserving strength) when the refractive index decreases from 2.5 (close to TiO_2) to 2 (close to Si_3N_4) (Figure S1).

Because of the RA, the wave propagating in the nanoresonator array established on the substrate (n = 1.46) reaches the diffraction limit; the black dashed line in Figure 1 represents the RA wavelength at $\lambda = p \times n = 350 \times 1.46 = 511$ nm, where p is the period of the array, and n is the refractive index of the resonators. In the region of wavelengths shorter than RA, the Mie lattice resonances can be suppressed because each Mie resonator does not couple with its neighbors. In the subdiffractional regime, zero-order reflection is suppressed because the nanoparticles in the array scatter light in different directions. For a wavelength longer than 511 nm, only zero-order light propagation occurs. Thus, the MDLR is stronger because the coupling of all resonators dominates and appears as a single peak in the reflection. When the refractive index of Mie resonators is 2.5, the shoulder of the MDLR is noticeable because of the weak Mie resonator−substrate coupling, and most of the mode energy is localized inside the resonator. Consequently, the lattice resonance from the substrate is not noticeable. When the refractive index of the resonator is 2, the mode profile spreads into the substrate, signifying strong coupling between the resonator and the substrate.[48,49] According to the comparison in Figure 1, a Si_3N_4 resonator engenders a sharper lattice resonance. In addition, Si_3N_4 is advantageous because of its high compatibility with the complementary metal−oxide−semiconductor process and its suitability for integrated photonics.

In this study, we developed a design approach involving the use of Si_3N_4 metasurfaces for realizing MDLR color pixels. We performed numerical analysis through full-wave simulations and experimentally demonstrated vivid color pixels afforded by the nanoparticle arrays with pure single-peak resonances. Compared with related concepts, the MDLR from the substrates could

https://dx.doi.org/10.1021/acsnano.0c00185
ACS Nano 2020, 14, 5678−5685

suppress high-order Mie resonances successfully through the RA at shorter wavelengths, thus enabling the creation of a highly saturated color without complex structures or design rules. By varying the size and period of nanostructure arrays, we generated vivid colors in both numerical simulations and experimental demonstrations. The color Si_3N_4 metasurfaces were determined to be effective for generating reflection images upon free-space excitation and for long-range dipole interactions when subjected to laterally incident light. These metasurfaces are thus suitable for waveguide applications in which light can propagate in compact and flat devices. The proposed phenomena and nanostructures are also applicable in integrated photonic devices. We expect that Si_3N_4 metasurfaces have considerable promise for application in eyewear displays and guided-wave illumination devices.

Si_3N_4 color pixels could be obtained using cubic arrays of varying nanoresonator width (w), interresonator gap (g), and

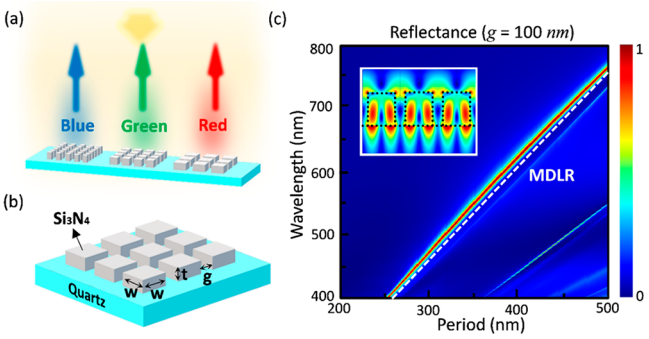

Figure 2. (a,b) Schematic of color pixel based on Si_3N_4 metasurfaces. In panel (a), the yellow arrow indicates the direction of the broadband incident light. (c) Simulated reflectance spectra with different periods (p) and widths ($w = p - 100$ nm). The thickness (t) of each cube is 270 nm. The inset presents the cross-section of Si_3N_4 nanoresonators (black dotted line) and the near-field distribution of the MDLR.

lattice period (p) (Figure 2a,b). These parameters are related as follows:

$$p = w + g \tag{1}$$

To excite an MDLR, the relevant MDR must be in the vicinity of the RA at longer wavelengths, as demonstrated by Babicheva et al.[41] The optical response of a dielectric nanostructure array can be approximated as a periodic electric and magnetic dipole coupling system. To avoid high-order Mie resonances and an EDR appearing in the reflectance spectrum, we designed the structure such that the EDR wavelength was shorter than the RA wavelength. Throughout the study, we maintained g at 100 nm for all Si_3N_4 metasurfaces under consideration to ensure that the EDR wavelength was shorter than the RA wavelength and that the MDR wavelength was longer than the RA wavelength in order to create robust MDLRs. Thus, the design rule for metasurfaces with MDLRs is expressed as follows:

$$p = w + 100\ \text{nm} \tag{2}$$

To create an appropriate cubic nanostructure in order to maintain the MDR as the width changes, we set the Si_3N_4 nanostructure thickness to 270 nm. Different Si_3N_4 nanostructure thickness may slightly change the baseline of the reflectance spectrum; nevertheless, because the reflectance spectrum was dominated by MDLRs, different Si_3N_4 thicknesses would not engender obvious changes in color. To calculate the reflectance of the metasurfaces, we used the finite-difference time-domain (FDTD) method implemented in the Lumerical software package (see Methods). The numerically derived reflectance of the Si_3N_4 metasurfaces with MDLRs is presented in Figure 2c. When the period (p) and width (w) of each Si_3N_4 metasurface were varied, the MDLR wavelength along with the RA wavelength shifted from 400 to 750 nm, covering the entire visible range.

Characterization. Figure 3a depicts scanning electron microscope (SEM) (FEI Helios G3CX) images of the Si_3N_4

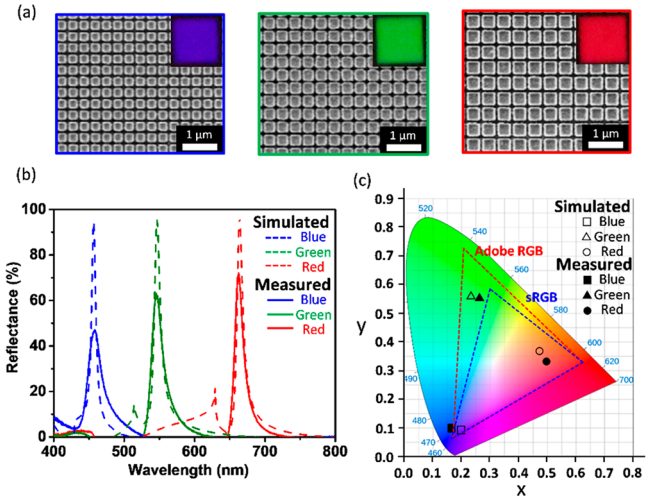

Figure 3. (a) SEM images of the Si_3N_4 color pixels with different periods and widths: the periods are 295, 355, and 435 nm (left to right). The insets are the optical reflection images. (b) Simulated and measured reflectance spectra of three-color pixels presented in panel (a). (c) Color gamut of Si_3N_4 metasurfaces, sRGB, and Adobe RGB color spaces in CIE 1931 chromaticity coordinates.

metasurfaces with different periods and widths. The insets present the optical image of each color pixel. Optical images were captured using an optical microscope (BX51, Olympus) with a 100× objective lens (LMPLFLN 5X BD, numerical aperture [NA] = 0.13). The spectra of color pixels were collected using a spectrometer (Kymera 193i, Andor) with a charge-coupled device (iVac 316 LDC-DD, Andor). The periods of blue, green, and red pixels fabricated in the study were 295, 355, and 435 nm, respectively (left to right, Figure 3a). The corresponding reflectance spectra in Figure 3b demonstrate suitable agreement between simulations and measurements. Because of the NA of the objective lens, the measured reflectance spectra were lower than ones obtained with the numerical simulation. The simulated and measured Si_3N_4 color pixels were plotted in CIE 1931 chromaticity coordinates for comparison with pixels plotted in the standard red−green−blue (sRGB) and Adobe RGB color spaces. For both the simulated and the measured pixels, the triangular area of the Si_3N_4 color pixels in CIE 1931 chromaticity coordinates could cover most of the sRGB and Adobe RGB color spaces, thus providing vivid colors.

To demonstrate the rich color features of Si_3N_4 color pixels, several possible color pixels are illustrated in Figure 4. Figure 4a depicts the optical images of different color pixels corresponding to array periods ranging from 295 to 435 nm. Figure 4b presents a comparison of the simulation and experimental results,

https://dx.doi.org/10.1021/acsnano.0c00185
ACS Nano 2020, 14, 5678−5685

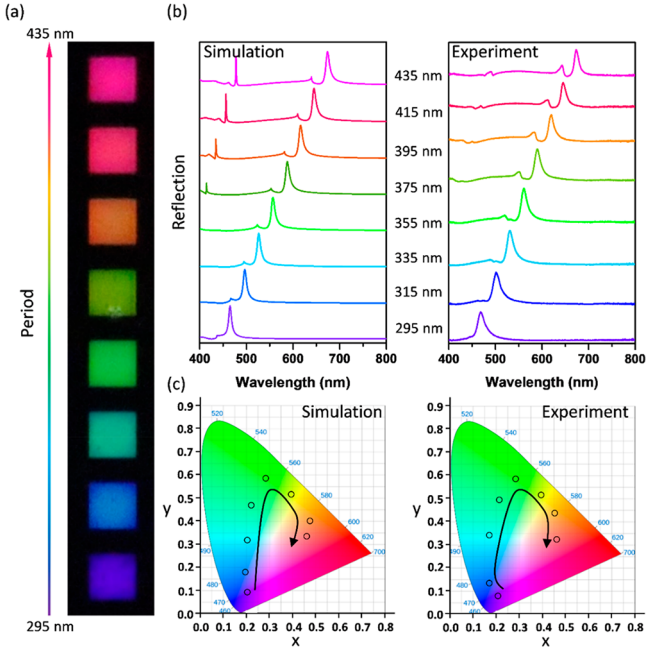

Figure 4. (a) Optical image of color pixels of the Si_3N_4 metasurfaces with different colors from blue (295 nm) to red (435 nm). (b) Simulated and measured reflectance spectra of corresponding color pixels in (a). (c) CIE 1931 chromaticity coordinates with different colors obtained in the simulations and experiments.

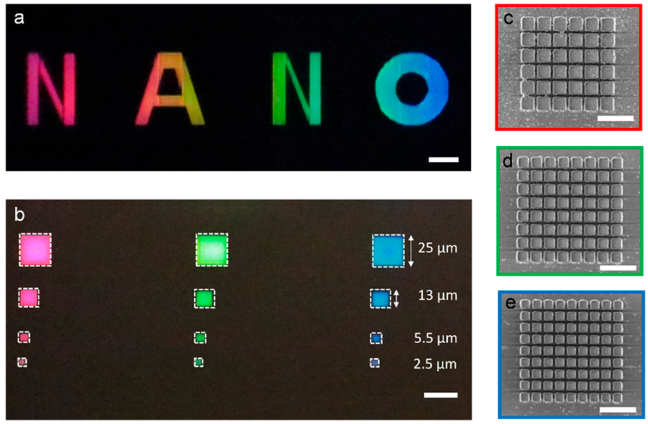

Figure 5. (a) Optical images of characters "NANO" created by gradually varying the size and period of Si_3N_4 color pixels. The scale bars are 10 μm. (b) Optical images of red, green, and blue Si_3N_4 metasurfaces of different areas: the lateral size changes from 25 to 2.5 μm, and the scale bar is 25 μm. Top-view SEM images for the 2.5 μm patterns with pixels (c) red, (d) green, and (e) blue in (b), and the scale bar is 1 μm.

indicating good agreement. For the red pixels, the peaks at relatively short wavelength ~450 nm are due to the lattice resonance of surrounding medium (n = 1) which are also close to the RA wavelength of the period in the air. However, this extra resonance peak is not apparent in the experiment due to the nonideal plane wave incidence from the objective lens (NA = 0.13). The color gamut obtained in the simulations and experiments is plotted in CIE 1931 chromaticity coordinates in Figure 4c. In the results, the colors are not affected much by the extra lattice resonances at the shorter wavelengths due to the low intensity.

The characters "NANO" presented in Figure 5a were fabricated using electron-beam lithography and Si_3N_4 metasurfaces with varying nanoresonator sizes and periods; the varying sizes and periods thus resulted in "NANO" being displayed in a rainbow-like color pattern. The different color pixel sizes, namely 25, 13, 5.5, and 2.5 μm, are presented in Figure 5b. This figure indicates that to obtain a high-resolution display using the vivid color pixels, the smallest Si_3N_4 metasurface that can be used should measure approximately 2.5 μm × 2.5 μm. The resolution can at least achieve about 10160 dpi with 2.5 μm × 2.5 μm pixels, which is sufficient for image or display applications. Furthermore, the pixels can also provide high saturated colors even when the numbers of periods are 6 × 6, 8 × 8, and 9 × 9 for red, green, and blue, respectively (Figure 5c,d,e). The angle-dependent properties of Si_3N_4 color pixels are investigated for both s- and p-polarization in Figures S3 and S4. The color of Si_3N_4 metasurfaces is approximately unaffected when the reflection angle is within ±30° in s-polarization (see Figure S5). According to the approximate field of view of an individual human eye, the symbol recognition viewing angle is about ±30°,[50] which means the Si_3N_4 color pixel in this report is adaptive for display application.

Lateral Incidence and Long-Range Dipole Interactions. To evaluate the potential applications of nanostructures in eyewear displays and integrated photonics, studying laterally incident light on Si_3N_4 metasurfaces is essential. Figure 6a illustrates schematics of the concept underlying laterally incident light on Si_3N_4 color pixels and the corresponding optical images. To demonstrate the concept, Figure 6b shows the image obtained after the characters "NANO" had been subjected to lateral light incidence. To accurately consider laterally incident light on an array structure, long-range dipole interactions between nanoresonators in the lattice must be considered. Schatz et al.[51,52] and Markel[53] have extensively investigated long-range dipole interactions in one-dimensional plasmonic chain structures; however, such interactions on dielectric metasurfaces have received less attention. Robust long-range dipole interactions can be observed by analyzing the spectrum of the extinction cross section of a nanostructure subjected to laterally incident light along the chain. The extinction cross section of each nanoresonator in a two-dimensional lattice or a one-dimensional chain can be considered an electric dipole or magnetic dipole and calculated as follows

$$C_{ext} = 4\pi k \mathrm{Im}\left(\frac{1}{1/\alpha_s - S}\right) \tag{3}$$

where S represents either the summation of retarded electric dipoles over the two-dimensional lattice (or one-dimensional chain) or the summation of retarded electric dipoles over magnetic dipoles, as expressed in the following equations, respectively:

$$S_{ED} = \sum_{j\neq i}\left[\frac{(1 - ikr_{ij})(3\cos^2\theta_{ij} - 1)e^{ikr_{ij}}}{r_{ij}^3} + \frac{k^2\sin^2\theta_{ij}e^{ikr_{ij}}}{r_{ij}}\right] \tag{4a}$$

$$S_{MD} = \sum_{j\neq i}\left[\frac{(1 - ikr_{ij})(3\sin^2\theta_{ij} - 1)e^{ikr_{ij}}}{r_{ij}^3} + \frac{k^2\cos^2\theta_{ij}e^{ikr_{ij}}}{r_{ij}}\right] \tag{4b}$$

https://dx.doi.org/10.1021/acsnano.0c00185
ACS Nano 2020, 14, 5678−5685

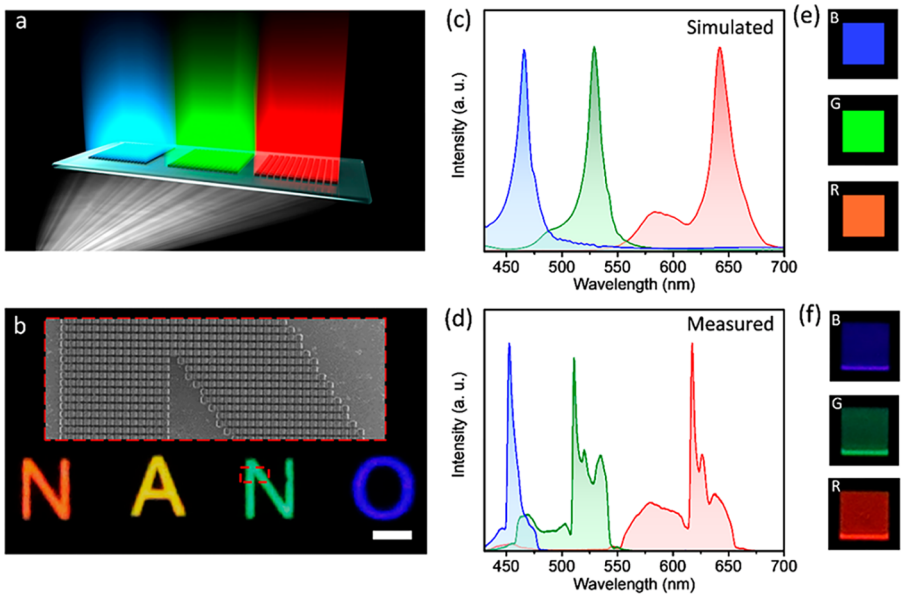

Figure 6. (a) Schematic of lateral light incidence on color pixels on Si_3N_4 metasurfaces. (b) Optical image of the characters "NANO" (scale bar is 25 μm). The inset presents the SEM image of a corner of the character "N". (c) Simulation and (d) experimental normalized extinction spectra collected above the Si_3N_4 metasurfaces with a thickness of 290 nm. The corresponding CIE color and measured optical image are shown on the right of simulated and measured spectra.

To approximate the shapes of nanoresonators using dielectric spheres, the polarizabilities of electric and magnetic dipoles in vacuum can be derived as follows

$$\alpha_{s,ED} = \frac{3a_1}{2k^3} \quad \text{and} \quad \alpha_{s,MD} = \frac{3b_1}{2k^3} \tag{5}$$

where k denotes the wavenumber of incident light with wavelength λ, and a_1 and b_1 denote the expansion coefficients in Mie theory associated with the fundamental electric and magnetic dipoles, respectively. For a two-dimensional lattice structure, to facilitate the realization of an efficient in-phase interaction of lattice nanoresonators, the array parameters and wavelength must satisfy the following condition

$$kr_{ij} = n2\pi \quad (\text{or alternatively } r_{ij} = n\lambda) \tag{6}$$

where n is an integer, and r_{ij} is the radius vector (spacing). Thus, the optimum spacing for the most robust in-phase interaction of electric dipoles is as follows

$$r_{ij} = \frac{n\lambda}{1 + \sin\theta} \tag{7}$$

where θ is the angle between the normal vector of the two-dimensional array and the wavevector of the incident light. For normal incidence (i.e., wavevector of incident light perpendicular to the surface of the two-dimensional array), the in-phase interaction is strongest if $r_{ij} = n\lambda$. By contrast, for lateral incidence (i.e., wavevector of the incident light parallel to the lattice vector of the two-dimensional array), the in-phase interaction is strongest if $r_{ij} = n\lambda/2$. The condition for lateral incidence resembles the antireflection condition for layer thickness in multilayer thin-film optics.

Figure 6c,d presents a robust long-range dipole interaction of periodic nanoresonators for a Si_3N_4 metasurface (see Methods). Measurement and simulation results revealed apparent and sharp peaks near the RA wavelength for the resonator lattice on the substrate. The images of bright color pixels with lateral incidence are shown in Figure 6e,f, and the corresponding CIE map is presented in Figure S6. In Figure S6, the Si_3N_4 color pixels with lateral incidence shows the large color space, which implies that the vivid colors can be achieved by lateral incidence. The experimental results also demonstrated a ripple beside the resonance peak (Figure 6d) that was caused by light propagating in the direction perpendicular to that of the incident light, a finding that is consistent with that demonstrated by a previous study.[51] As shown in Figure 6c, the ripple was not observed because compared with the experiments, the simulations had a lower number of nanoresonators in which light propagated in the direction perpendicular to that of the incident light. In the simulations, the numbers of nanoresonators on the color pixel metasurface were 50 and 16 in the x- and y-directions, respectively (Figures S7 and S8). In the experiment, the red pixel (Figure 3a) comprised 230 nanoresonators in each direction, corresponding to a total lateral size of approximately 100 μm.

Notably, Figure 6 shows results obtained for transverse magnetic (TM) polarization, in which the electric field is typically perpendicular to the plane of the color pixel. In transverse electric (TE) polarization, in which the magnetic field is perpendicular to the plane of the color pixel, the optical image is dark, and no resonance can be observed in the spectrum upon such lateral incidence (Figure S9). Previous research also reported selective properties of two-dimensional arrays subjected to lateral incidence under TM and TE polarizations.[51] In a Si_3N_4 nanophotonic system, the TE and TM modes of a waveguide can arbitrarily be switched by system elements such as polarization rotator-splitters.[54,55] The switching of color pixels can be implemented through a Gaussian light source that includes a waveguide with laterally incident light by a polarization rotator; such designs can also be applied in eyewear devices. If a polarization rotator is not used, scattering signals would still exhibit a high polarization ratio, and the corresponding metasurface can be combined with a liquid crystal device or polarizer for application in the active color displays (Figure S10).

https://dx.doi.org/10.1021/acsnano.0c00185
ACS Nano 2020, 14, 5678−5685

CONCLUSIONS

In this study, we numerically designed and experimentally demonstrated vivid color pixels on Si_3N_4 metasurfaces. To create vivid color pixels, resonance peaks in spectra could be identified by exciting MDLRs in nanoresonator periodic arrays. We experimentally demonstrated that color pixels could be easily generated using a single-layer metasurface without a sophisticated design involving a multilayer structure. For applications in display equipment, the minimum color pixel size can be 2.5 μm × 2.5 μm, thus the resolution can achieve about 10160 dpi. Lattice resonances were demonstrated under conditions that involved laterally incident light (along the array plane), indicating the effectiveness of the Si_3N_4 metasurfaces in eyewear displays and guided-wave illumination techniques. Furthermore, pixel switching could be achieved through the selective properties of TM and TE polarizations. Comparing Si_3N_4 color pixels with those rendered in the sRGB and Adobe RGB color spaces, we observed that most of the color spaces could be covered by the Si_3N_4 color pixels in both normal and lateral incidence. In addition, the proposed metasurface design approach based on MDLR excitation can be applied to other high-refractive-index materials with low optical loss, such as Ge and GaN in the infrared spectral range. Not only the structural imprint but also the dynamic displays with colorful metasurfaces could be achieved by combining lattice resonance and with different kinds of the surrounding mediums, *e.g.*, liquid crystals,[56] mixing colors,[57] different gases[47,58,59] or solutions,[45,60] *etc.* We believe that Si_3N_4 color pixels can be utilized in traditional displays or eyewear devices in the future.

METHODS

Fabrication. An electron beam lithography system (ELS-7500 EX by ELIONIX) was used to fabricate Si_3N_4 metasurfaces. A Si_3N_4 thin film (thickness = 270 nm) was deposited on quartz substrates through a plasma-enhanced chemical vapor deposition system (Oxford Plasmalab System 100). Subsequently, a poly(methyl methacrylate) (PMMA)-A4 photoresist was spin-coated on the Si_3N_4 thin film for pattern definition. A conductive polymer (AR-PC 5090 by ALLRESIST) was spin-coated on the PMMA photoresist to avoid charge accumulation. Electron beam lithography was then used to expose the array of rectangles. To form a resist mask, chromium layers (thickness = 20 nm) were deposited on a patterned Si_3N_4 thin film. A lift-off process was used to form a chromium rectangular array. To fabricate the Si_3N_4 cubic column, an inductively coupled plasma etching system (EIS-700 by ELIONIX) was used to etch the Si_3N_4 layer. Finally, the chromium hat was removed through wet etching.

Simulation for Normal Incidence. The FDTD method (Lumerical FDTD) was used to calculate the reflectance spectra and electric field distributions around nanoparticles in the array. The Si_3N_4 metasurface on the quartz substrate was illuminated by a plane wave source in the *z*-direction to excite Mie lattice resonances. Reflection signals were collected using a monitor placed on top of the Si_3N_4 metasurface and behind the plane wave source. To avoid signal reflection from boundaries, perfectly matching layers were applied to the boundaries in the *z*-direction. To create a periodic structure, boundaries in the *x*- and *y*-directions were set to satisfy Bloch's condition.

Simulation for Lateral Incidence. The FDTD method (Lumerical FDTD) was used to collect extinction spectra for the top of the metasurfaces. Each Si_3N_4 metasurface was positioned next to the Si_3N_4 waveguide serving as a laterally incident light source. To simulate light from the waveguide, the propagation mode of the waveguide was set to the fundamental TE mode. The Si_3N_4 metasurface array comprised 50 units/nanoresonators in the light propagation direction and 16 units/nanoresonators in the direction perpendicular to the light propagation direction. Extinction signals were collected using a power monitor placed at a distance of 124 μm above the metasurface.

Measurement for Lateral Incidence. A laterally incident light source passed through a collimated lens was set next to the Si_3N_4 metasurface. Extinction signals were collected using an optical microscope (BX51, Olympus) with an objective lens (LMPLFLN 5X BD, NA = 0.13). The collected light was analyzed using a spectrometer (Kymera 193i, Andor) with a charge-coupled device (iVac 316 LDC-DD, Andor).

ASSOCIATED CONTENT

Supporting Information

The Supporting Information is available free of charge at https://pubs.acs.org/doi/10.1021/acsnano.0c00185.

Figures: (S1) refractive index of Si_3N_4 and TiO_2; (S2) fabrication processes of Si_3N_4 metasurfaces; (S3) oblique reflection of Si_3N_4 color pixels under *s*- and *p*-polarization for thickness of 270 nm; (S4) oblique reflection of Si_3N_4 color pixels under *s*- and *p*-polarization for thickness of 180 nm; (S5) images of Si_3N_4 color pixels with different viewing angles; (S6) CIE map of Si_3N_4 color pixels with lateral incidence; (S7) ripples in scattering spectrum with lateral incidence; (S8) schematics of waveguides with tapers and color metasurfaces in FDTD simulations; (S9) optical images of color pixels with lateral incidence of TM and TE polarization; and (S10) optical images for TM incidence and analysis in *y*- and *x*-polarizations (PDF)

AUTHOR INFORMATION

Corresponding Author

Kuo-Ping Chen − *Institute of Imaging and Biomedical Photonics, College of Photonics, National Chiao-Tung University, Tainan 71150, Taiwan;* orcid.org/0000-0001-6256-9145; Email: kpchen@nctu.edu.tw

Authors

Jhen-Hong Yang − *Institute of Photonic System, College of Photonics, National Chiao-Tung University, Tainan 71150, Taiwan;* orcid.org/0000-0003-3176-5009

Viktoriia E. Babicheva − *Department of Electrical and Computer Engineering, University of New Mexico, Albuquerque, New Mexico 87131, United States;* orcid.org/0000-0002-0789-5738

Min-Wen Yu − *Institute of Lighting and Energy Photonics, College of Photonics, National Chiao-Tung University, Tainan 71150, Taiwan;* orcid.org/0000-0003-4173-8813

Tien-Chang Lu − *Department of Photonics, College of Electrical and Computer Engineering, National Chiao-Tung University, Hsinchu 30010, Taiwan;* orcid.org/0000-0003-4192-9919

Tzy-Rong Lin − *Department of Mechanical and Mechatronic Engineering and Center of Excellence for Ocean Engineering, National Taiwan Ocean University, Keelung 20224, Taiwan*

Complete contact information is available at: https://pubs.acs.org/10.1021/acsnano.0c00185

Author Contributions

J.-H.Y. performed the sample fabrication, simulation, and optical characterization. V.B. and J.-H.Y. conducted the theory model. M.-W.Y. conducted the SEM images. M.-W.Y., V.B., K.-P. C., T.-R. L., and T.-C. L. helped in analyzing the experimental data. J.-H.Y. and K.-P.C. wrote the manuscript. All authors discussed the results and commented on the manuscript.

https://dx.doi.org/10.1021/acsnano.0c00185
ACS Nano 2020, 14, 5678−5685

Notes

The authors declare no competing financial interest.

ACKNOWLEDGMENTS

The authors would like to thank Vishal Vashistha's initial simulation/discussion and Ji-Ren Ku's effort on taking high-resolution SEM images. This work was supported by the Higher Education Sprout Project of the National Chiao Tung University and Ministry of Education and the Ministry of Science and Technology (MOST-107-2221-E-009-046-MY3; 107-2218-E-009-056; 108-2923-E-009-003-MY3). V.B. acknowledges support from the Air Force Office of Scientific Research under Grant No. FA9550-19-1-0032.

REFERENCES

(1) Su, V.-C.; Chu, C. H.; Sun, G.; Tsai, D. P. Advances in Optical Metasurfaces: Fabrication and Applications. *Opt. Express* **2018**, *26*, 13148−13182.
(2) Højlund-Nielsen, E.; Clausen, J.; Mäkela, T.; Thamdrup, L. H.; Zalkovskij, M.; Nielsen, T.; Li Pira, N.; Ahopelto, J.; Mortensen, N. A.; Kristensen, A. Plasmonic Colors: Toward Mass Production of Metasurfaces. *Adv. Mater. Technol.* **2016**, *1*, 1600054.
(3) Colburn, S.; Zhan, A.; Majumdar, A. Metasurface Optics for Full-Color Computational Imaging. *Sci. Adv.* **2018**, *4*, No. eaar2114.
(4) Song, M.; Wang, D.; Peana, S.; Choudhury, S.; Nyga, P.; Kudyshev, Z. A.; Yu, H.; Boltasseva, A.; Shalaev, V. M.; Kildishev, A. V. Colors with Plasmonic Nanostructures: A Full-Spectrum Review. *Appl. Phys. Rev.* **2019**, *6*, 041308.
(5) Duan, X.; Kamin, S.; Liu, N. Dynamic Plasmonic Colour Display. *Nat. Commun.* **2017**, *8*, 14606.
(6) Zeng, B.; Gao, Y.; Bartoli, F. J. Ultrathin Nanostructured Metals for Highly Transmissive Plasmonic Subtractive Color Filters. *Sci. Rep.* **2013**, *3*, 2840.
(7) Kristensen, A.; Yang, J. K.; Bozhevolnyi, S. I.; Link, S.; Nordlander, P.; Halas, N. J.; Mortensen, N. A. Plasmonic Colour Generation. *Nat. Rev. Mater.* **2017**, *2*, 16088.
(8) Franklin, D.; Chen, Y.; Vazquez-Guardado, A.; Modak, S.; Boroumand, J.; Xu, D.; Wu, S.-T.; Chanda, D. Polarization-Independent Actively Tunable Colour Generation on Imprinted Plasmonic Surfaces. *Nat. Commun.* **2015**, *6*, 7337.
(9) Rezaei, S. D.; Hong Ng, R. J.; Dong, Z.; Ho, J.; Koay, E. H.; Ramakrishna, S.; Yang, J. K. Wide-Gamut Plasmonic Color Palettes with Constant Subwavelength Resolution. *ACS Nano* **2019**, *13*, 3580−3588.
(10) Xie, Z.-W.; Yang, J.-H.; Vashistha, V.; Lee, W.; Chen, K.-P. Liquid-Crystal Tunable Color Filters Based on Aluminum Metasurfaces. *Opt. Express* **2017**, *25*, 30764−30770.
(11) Yun, J.-G.; Sung, J.; Kim, S.-J.; Yun, H.; Choi, C.; Lee, B. Ultracompact Meta-Pixels for High Colour Depth Generation Using a Bi-Layered Hybrid Metasurface. *Sci. Rep.* **2019**, *9*, 15381.
(12) Lin, R. J.; Su, V.-C.; Wang, S.; Chen, M. K.; Chung, T. L.; Chen, Y. H.; Kuo, H. Y.; Chen, J.-W.; Chen, J.; Huang, Y.-T. Achromatic Metalens Array for Full-Colour Light-Field Imaging. *Nat. Nanotechnol.* **2019**, *14*, 227.
(13) Chen, B. H.; Wu, P. C.; Su, V.-C.; Lai, Y.-C.; Chu, C. H.; Lee, I. C.; Chen, J.-W.; Chen, Y. H.; Lan, Y.-C.; Kuan, C.-H. Gan Metalens for Pixel-Level Full-Color Routing at Visible Light. *Nano Lett.* **2017**, *17*, 6345−6352.
(14) Sun, S.; Zhou, Z.; Zhang, C.; Gao, Y.; Duan, Z.; Xiao, S.; Song, Q. All-Dielectric Full-Color Printing with TiO_2 Metasurfaces. *ACS Nano* **2017**, *11*, 4445−4452.
(15) Khorasaninejad, M.; Zhu, A. Y.; Roques-Carmes, C.; Chen, W. T.; Oh, J.; Mishra, I.; Devlin, R. C.; Capasso, F. Polarization-Insensitive Metalenses at Visible Wavelengths. *Nano Lett.* **2016**, *16*, 7229−7234.
(16) Genevet, P.; Capasso, F.; Aieta, F.; Khorasaninejad, M.; Devlin, R. Recent Advances in Planar Optics: From Plasmonic to Dielectric Metasurfaces. *Optica* **2017**, *4*, 139−152.
(17) Højlund-Nielsen, E.; Weirich, J.; Nørregaard, J.; Garnaes, J.; Mortensen, N. A.; Kristensen, A. Angle-Independent Structural Colors of Silicon. *J. Nanophotonics* **2014**, *8*, 083988.
(18) Dong, Z.; Ho, J.; Yu, Y. F.; Fu, Y. H.; Paniagua-Dominguez, R.; Wang, S.; Kuznetsov, A. I.; Yang, J. K. Printing beyond sRGB Color Gamut by Mimicking Silicon Nanostructures in Free-Space. *Nano Lett.* **2017**, *17*, 7620−7628.
(19) Zhu, X.; Yan, W.; Levy, U.; Mortensen, N. A.; Kristensen, A. Resonant Laser Printing of Structural Colors on High-Index Dielectric Metasurfaces. *Sci. Adv.* **2017**, *3*, No. e1602487.
(20) Kuznetsov, A. I.; Miroshnichenko, A. E.; Brongersma, M. L.; Kivshar, Y. S.; Luk'yanchuk, B. Optically Resonant Dielectric Nanostructures. *Science* **2016**, *354*, No. aag2472.
(21) Park, C.-S.; Koirala, I.; Gao, S.; Shrestha, V. R.; Lee, S.-S.; Choi, D.-Y. Structural Color Filters Based on an All-Dielectric Metasurface Exploiting Silicon-Rich Silicon Nitride Nanodisks. *Opt. Express* **2019**, *27*, 667−679.
(22) Yu, Y. F.; Zhu, A. Y.; Paniagua-Domínguez, R.; Fu, Y. H.; Luk'yanchuk, B.; Kuznetsov, A. I. High-Transmission Dielectric Metasurface with 2π Phase Control at Visible Wavelengths. *Laser Photonics Rev.* **2015**, *9*, 412−418.
(23) Decker, M.; Staude, I.; Falkner, M.; Dominguez, J.; Neshev, D. N.; Brener, I.; Pertsch, T.; Kivshar, Y. S. High-Efficiency Dielectric Huygens' Surfaces. *Adv. Opt. Mater.* **2015**, *3*, 813−820.
(24) Staude, I.; Miroshnichenko, A. E.; Decker, M.; Fofang, N. T.; Liu, S.; Gonzales, E.; Dominguez, J.; Luk, T. S.; Neshev, D. N.; Brener, I. Tailoring Directional Scattering through Magnetic and Electric Resonances in Subwavelength Silicon Nanodisks. *ACS Nano* **2013**, *7*, 7824−7832.
(25) Evlyukhin, A. B.; Reinhardt, C.; Evlyukhin, E.; Chichkov, B. N. Multipole Analysis of Light Scattering by Arbitrary-Shaped Nanoparticles on a Plane Surface. *J. Opt. Soc. Am. B* **2013**, *30*, 2589−2598.
(26) Nagasaki, Y.; Hotta, I.; Suzuki, M.; Takahara, J. Metal-Masked Mie-Resonant Full-Color Printing for Achieving Free-Space Resolution Limit. *ACS Photonics* **2018**, *5*, 3849−3855.
(27) Nagasaki, Y.; Suzuki, M.; Takahara, J. All-Dielectric Dual-Color Pixel with Subwavelength Resolution. *Nano Lett.* **2017**, *17*, 7500−7506.
(28) Proust, J.; Bedu, F. d. r.; Gallas, B.; Ozerov, I.; Bonod, N. All-Dielectric Colored Metasurfaces with Silicon Mie Resonators. *ACS Nano* **2016**, *10*, 7761−7767.
(29) Flauraud, V.; Reyes, M.; Paniagua-Dominguez, R.; Kuznetsov, A. I.; Brugger, J. Silicon Nanostructures for Bright Field Full Color Prints. *ACS Photonics* **2017**, *4*, 1913−1919.
(30) Yang, B.; Liu, W.; Li, Z.; Cheng, H.; Choi, D.-Y.; Chen, S.; Tian, J. Ultra-Highly Saturated Structural Colors Enhanced by Multipolar-Modulated Metasurfaces. *Nano Lett.* **2019**, *19*, 4221−4228.
(31) Auguié, B.; Barnes, W. L. Collective Resonances in Gold Nanoparticle Arrays. *Phys. Rev. Lett.* **2008**, *101*, 143902.
(32) Evlyukhin, A. B.; Reinhardt, C.; Zywietz, U.; Chichkov, B. N. Collective Resonances in Metal Nanoparticle Arrays with Dipole-Quadrupole Interactions. *Phys. Rev. B: Condens. Matter Mater. Phys.* **2012**, *85*, 245411.
(33) Zhou, W.; Dridi, M.; Suh, J. Y.; Kim, C. H.; Co, D. T.; Wasielewski, M. R.; Schatz, G. C.; Odom, T. W. Lasing Action in Strongly Coupled Plasmonic Nanocavity Arrays. *Nat. Nanotechnol.* **2013**, *8*, 506.
(34) Thackray, B. D.; Thomas, P. A.; Auton, G. H.; Rodriguez, F. J.; Marshall, O. P.; Kravets, V. G.; Grigorenko, A. N. Super-Narrow, Extremely High Quality Collective Plasmon Resonances at Telecom Wavelengths and Their Application in a Hybrid Graphene-Plasmonic Modulator. *Nano Lett.* **2015**, *15*, 3519−3523.
(35) Swiecicki, S. D.; Sipe, J. Surface-Lattice Resonances in Two-Dimensional Arrays of Spheres: Multipolar Interactions and a Mode Analysis. *Phys. Rev. B: Condens. Matter Mater. Phys.* **2017**, *95*, 195406.
(36) Wang, W.; Ramezani, M.; Väkeväinen, A. I.; Törmä, P.; Rivas, J. G.; Odom, T. W. The Rich Photonic World of Plasmonic Nanoparticle Arrays. *Mater. Today* **2018**, *21*, 303−314.

https://dx.doi.org/10.1021/acsnano.0c00185
ACS Nano 2020, 14, 5678−5685

(37) Kravets, V. G.; Kabashin, A. V.; Barnes, W. L.; Grigorenko, A. N. Plasmonic Surface Lattice Resonances: A Review of Properties and Applications. *Chem. Rev.* **2018**, *118*, 5912−5951.
(38) Baur, S.; Sanders, S.; Manjavacas, A. Hybridization of Lattice Resonances. *ACS Nano* **2018**, *12*, 1618−1629.
(39) Zakomirnyi, V.; Ershov, A.; Gerasimov, V.; Karpov, S.; Ågren, H.; Rasskazov, I. Collective Lattice Resonances in Arrays of Dielectric Nanoparticles: A Matter of Size. *Opt. Lett.* **2019**, *44*, 5743−5746.
(40) Zakomirnyi, V. I.; Karpov, S. V.; Ågren, H.; Rasskazov, I. L. Collective Lattice Resonances in Disordered and Quasi-Random All-Dielectric Metasurfaces. *J. Opt. Soc. Am. B* **2019**, *36*, E21−E29.
(41) Babicheva, V. E.; Evlyukhin, A. B. Resonant Lattice Kerker Effect in Metasurfaces with Electric and Magnetic Optical Responses. *Laser Photonics Rev.* **2017**, *11*, 1700132.
(42) Evlyukhin, A. B.; Reinhardt, C.; Seidel, A.; Luk'yanchuk, B. S.; Chichkov, B. N. Optical Response Features of Si-Nanoparticle Arrays. *Phys. Rev. B: Condens. Matter Mater. Phys.* **2010**, *82*, 045404.
(43) Yang, C.-Y.; Yang, J.-H.; Yang, Z.-Y.; Zhou, Z.-X.; Sun, M.-G.; Babicheva, V. E.; Chen, K.-P. Nonradiating Silicon Nanoantenna Metasurfaces as Narrowband Absorbers. *ACS Photonics* **2018**, *5*, 2596−2601.
(44) Babicheva, V. E.; Petrov, M. I.; Baryshnikova, K. V.; Belov, P. A. Reflection Compensation Mediated by Electric and Magnetic Resonances of All-Dielectric Metasurfaces. *J. Opt. Soc. Am. B* **2017**, *34*, D18−D28.
(45) Sun, S.; Yang, W.; Zhang, C.; Jing, J.; Gao, Y.; Yu, X.; Song, Q.; Xiao, S. Real-Time Tunable Colors from Microfluidic Reconfigurable All-Dielectric Metasurfaces. *ACS Nano* **2018**, *12*, 2151−2159.
(46) Zhang, C.; Jing, J.; Wu, Y.; Fan, Y.; Yang, W.; Wang, S.; Song, Q.; Xiao, S. Stretchable All-Dielectric Metasurfaces with Polarization-Insensitive and Full-Spectrum Response. *ACS Nano* **2020**, *14*, 1418−1426.
(47) Wu, Y.; Yang, W.; Fan, Y.; Song, Q.; Xiao, S. TiO_2 Metasurfaces: From Visible Planar Photonics to Photochemistry. *Sci. Adv.* **2019**, *5*, No. eaax0939.
(48) Zhang, S.; Bao, K.; Halas, N. J.; Xu, H.; Nordlander, P. Substrate-Induced Fano Resonances of a Plasmonic Nanocube: A Route to Increased-Sensitivity Localized Surface Plasmon Resonance Sensors Revealed. *Nano Lett.* **2011**, *11*, 1657−1663.
(49) Auguié, B.; Bendana, X. M.; Barnes, W. L.; de Abajo, F. J. G. Diffractive Arrays of Gold Nanoparticles Near an Interface: Critical Role of the Substrate. *Phys. Rev. B: Condens. Matter Mater. Phys.* **2010**, *82*, 155447.
(50) Traquair, H. M. Chapter 1. *An Introduction to Clinical Perimetry*, 6th ed.; Henry Kimpton: London, 1938; pp 4−16.
(51) Zou, S.; Schatz, G. C. Theoretical Studies of Plasmon Resonances in One-Dimensional Nanoparticle Chains: Narrow Lineshapes with Tunable Widths. *Nanotechnology* **2006**, *17*, 2813.
(52) Zou, S.; Janel, N.; Schatz, G. C. Silver Nanoparticle Array Structures That Produce Remarkably Narrow Plasmon Lineshapes. *J. Chem. Phys.* **2004**, *120*, 10871−10875.
(53) Markel, V. A. Divergence of Dipole Sums and the Nature of Non-Lorentzian Exponentially Narrow Resonances in One-Dimensional Periodic Arrays of Nanospheres. *J. Phys. B: At., Mol. Opt. Phys.* **2005**, *38*, L115.
(54) Sacher, W. D.; Barwicz, T.; Taylor, B. J.; Poon, J. K. Polarization Rotator-Splitters in Standard Active Silicon Photonics Platforms. *Opt. Express* **2014**, *22*, 3777−3786.
(55) Sacher, W. D.; Huang, Y.; Ding, L.; Barwicz, T.; Mikkelsen, J. C.; Taylor, B. J.; Lo, G.-Q.; Poon, J. K. Polarization Rotator-Splitters and Controllers in a Si_3N_4-on-SOI Integrated Photonics Platform. *Opt. Express* **2014**, *22*, 11167−11174.
(56) Franklin, D.; Chen, Y.; Vazquez-Guardado, A.; Modak, S.; Boroumand, J.; Xu, D.; Wu, S.-T.; Chanda, D. Polarization-Independent Actively Tunable Colour Generation on Imprinted Plasmonic Surfaces. *Nat. Commun.* **2015**, *6*, 7337.
(57) Gao, Y.; Huang, C.; Hao, C.; Sun, S.; Zhang, L.; Zhang, C.; Duan, Z.; Wang, K.; Jin, Z.; Zhang, N. Lead Halide Perovskite Nanostructures for Dynamic Color Display. *ACS Nano* **2018**, *12*, 8847−8854.
(58) Chen, Y.; Duan, X.; Matuschek, M.; Zhou, Y.; Neubrech, F.; Duan, H.; Liu, N. Dynamic Color Displays Using Stepwise Cavity Resonators. *Nano Lett.* **2017**, *17*, 5555−5560.
(59) Duan, X.; Kamin, S.; Liu, N. Dynamic Plasmonic Colour Display. *Nat. Commun.* **2017**, *8*, 14606.
(60) Daqiqeh Rezaei, S.; Ho, J.; Naderi, A.; Tavakkoli Yaraki, M.; Wang, T.; Dong, Z.; Ramakrishna, S.; Yang, J. K. Tunable, Cost-Effective, and Scalable Structural Colors for Sensing and Consumer Products. *Adv. Opt. Mater.* **2019**, *7*, 1900735.

https://dx.doi.org/10.1021/acsnano.0c00185
ACS Nano 2020, 14, 5678−5685